Potential Energy Surfaces for Ring-Rearrangement Processes in Tricarbonyl(cyclooctatetraene)chromium(0)

Michael S. Lawless and Dennis S. Marynick*

Contribution from the Department of Chemistry, University of Texas at Arlington, Arlington, Texas 76019-0065. *Received November 1, 1990*

Abstract: Potential energy surfaces have been calculated for fluxional processes exhibited by $(CO)_3(\eta^6\text{-}C_8H_8)Cr$. The geometry of the ground state, two "piano-stool" structures, and points along the surfaces in the 1,2-, 1,3-, 1,4-, and 1,5-shifts were fully optimized with the partial retention of diatomic differential overlap (PRDDO) method. Ab initio molecular orbital calculations with large basis sets were then performed on the estimated transition states for each of the above surfaces in order to evaluate the energetics. The calculated activation energies at the ab initio level are 6.3, 0.6, 10.0, and 11.6 kcal/mol for the 1,2-, 1,3-, 1,4-, and 1,5-shifts, respectively. A larger basis set, including polarization functions on the cyclooctatetraene ring, yields calculated values of 8.9 and 2.9 kcal/mol for the 1,2- and 1,3-shifts, respectively. The piano-stool structure in which all the R(C–C) distances and the R(Cr–C) distances are equal, which is generally assumed to be the transition state in the random-shift mechanism, is 17.6 kcal/mol higher in energy than the ground state. The lowest energy pathway is the 1,3-shift, in agreement with experiment. The estimated transition state for this pathway is a 16-electron complex in which the ring is η^4-bound to chromium. The next lowest energy pathway is the 1,2-shift. The transition state on this surface contains an η^5-bound cyclooctatetraene ring.

Introduction

During the last three decades, extensive studies have been conducted on the fluxional behavior of organometallic compounds. Experimental investigations have yielded a great deal of information on the thermodynamic and mechanistic aspects of stereochemically nonrigid molecules.[1] Yet, relatively few computational studies have been published on this subject, mainly due to the large size and electronic complexities of these systems and the difficulties involved in locating transition states. One of the most common types of fluxionality is the scrambling of the equatorial and axial ligands in trigonal-bipyramidal complexes. Koga et al. have studied this type of rearrangement in $(H)(C_2H_4)(CO)_2(PH_3)Rh$ with ab initio theory and concluded that a Berry pseudorotation is the operative mechanism.[2] Hansen and Marynick have explored the potential energy surfaces for several plausible mechanisms of cis–trans isomerization in $R(CO)_5Cr$ (R = CO, phosphine, and triphenylphosphine).[3] They have also investigated the η^1 to η^5 conversion of the cyclopentadienyl (Cp) ligands in chlorotris(cyclopentadienyl)titanium(IV).[4] Mann has developed a qualitative theory that can predict trends in stereochemically nonrigid systems.[5] Albright and Hoffmann have examined a wide array of systems using qualitative molecular orbital theory.[6] These have included rearrangements that require the breaking and forming of chemical bonds as well as studies of rotational barriers and conformational preferences.

The fluxional behavior of cyclooctatetraene (COT) systems is extremely diverse owing to the fact that its modes of binding to a metal can vary in several different ways. When it is bound in an η^2 fashion, as in $Mn(CO)_2(\eta^2\text{-COT})(\eta^5\text{-Cp})$[7] or $[(\eta^5\text{-Cp})(\eta^2\text{-COT})Fe]^+$,[8] the ring is static. In contrast, η^4-COT rings are highly fluxional. For example, the activation energy for 1,2-shifts in $(CO)_3(\eta^4\text{-COT})Fe$ is 8.1 kcal/mol.[9] Another fascinating compound in the cyclooctatetraene family is $(\eta^4\text{-COT})(\eta^6\text{-COT})Fe$. This molecule not only exhibits ring whizzing but also an η^4 to η^6 conversion.[10] The fluxional behavior of an η^6-COT ring depends on the molecular environment. For example, in $(\eta^6\text{-COT})(\eta^4\text{-COD})Os$ (COD = cycloocta-1,5-diene) rearrangement occurs via 1,5-shifts,[11] which is unusual because the majority of cyclic olefins rearrange by simple 1,2-shifts.[1] When COT is bound to Fe^{2+}, as in $[Fe(\eta^5\text{-Cp})(\eta^6\text{-COT})]^+$, the ring is not fluxional at 35 °C.[12]

Tricarbonyl(η^6-cyclooctatetraene)chromium(0) has had a long history of experimental studies aimed at understanding its fluxional behavior. Evidence of fluxionality in this system was first obtained in 1966 by Kreiter, who estimated the rate of rearrangement to be approximately 25 s^{-1} at 20 °C with a free energy of activation equal to 15.4 kcal/mol.[13] Not much could be said about the ring-shift mechanism in this early study because the proton NMR spectra were too complex. This was due to spin–spin coupling of adjacent protons in the ring. To circumvent this problem, Cotton et al. employed $(CO)_3(TMCOT)M$ (M = Cr, Mo, W; TMCOT = 1,3,5,7-tetramethylcyclooctatetraene).[14] In these molecules, the ring protons are separated by methyl groups on adjacent carbon atoms so that line-shape analysis can be performed. The activation energy was determined to be 16.0 kcal/mol for M = Cr and Mo in the slow-rearrangement phase. The rearrangement occurred via a 1,2-shift mechanism. In 1974, Cotton confirmed his previous findings on $(CO)_3(TMCOT)M$ using ^{13}C NMR spectroscopy and showed that, in contrast, $(CO)_3(COT)M$ (M = Cr, Mo, W) rearranges via a 1,3- or random-shift mechanism.[15] While NMR line-broadening experiments cannot distinguish between these two mechanisms, it was argued that random shifts rather than 1,3-shifts were occurring.

(1) Mann, B. E. In *Comprehensive Organometallic Chemistry*; Abel, E. W., Stone, F. G. A., Wilkinson, G., Eds.; Pergamon Press: Oxford, U.K., 1982; Vol. 3, pp 89–171.
(2) Koga, N.; Jin, S. Q.; Morokuma, K. *J. Am. Chem. Soc.* **1988**, *110*, 3417.
(3) Hansen, L. M.; Marynick, D. S. *Inorg. Chem.* **1990**, *29*, 2482. See also: Marynick, D. S.; Askari, S.; Nickerson, D. F. *Inorg. Chem.* **1985**, *24*, 868.
(4) Hansen, L. M.; Marynick, D. S. *J. Am. Chem. Soc.* **1988**, *110*, 2358.
(5) Mann, B. E. *Chem. Soc. Rev.* **1986**, *15*, 167.
(6) (a) Kang, S.; Albright, T. A.; Mealli, C. *Inorg. Chem.* **1987**, *26*, 3158. (b) Mlekuz, M.; Bougeard, P.; Sayer, B. G.; McGlinchey, M. J.; Rodger, C. A.; Churchill, M. R.; Ziller, J. W.; Kang, S.; Albright, T. A. *Organometallics* **1986**, *5*, 1656. (c) Reynolds, S. D.; Albright, T. A. *Organometallics* **1985**, *4*, 980. (d) Silvestre, J.; Albright, T. A. *J. Am. Chem. Soc.* **1985**, *107*, 6829. (e) Albright, T. A.; Hofmann, P.; Hoffmann, R.; Lillya, C. P.; Dobosh, P. A. *J. Am. Chem. Soc.* **1983**, *105*, 3396. (f) Albright, T. A. *Acc. Chem. Res.* **1982**, *15*, 149. (g) Karel, K. J.; Albright, T. A.; Brookhart, M. *Organometallics* **1982**, *1*, 419. (h) Hoffmann, R. *Science* **1981**, *211*, 995. (i) Albright, T. A.; Hoffmann, R.; Thibeault, J. C.; Thorn, D. L. *J. Am. Chem. Soc.* **1979**, *101*, 3801. (j) Albright, T. A.; Hoffmann, R.; Tse, Y.; D'Ottavio, T. *J. Am. Chem. Soc.* **1979**, *101*, 3812. (k) Albright, T. A.; Hoffmann, R. *Chem. Ber.* **1978**, *111*, 1591. (l) Albright, T. A.; Hofmann, P.; Hoffmann, R. *J. Am. Chem. Soc.* **1977**, *99*, 7546.
(7) Benson, I. B.; Knox, S. A. R.; Stansfield, R. F. D.; Woodward, P. *J. Chem. Soc., Chem. Commun.* **1977**, 404.
(8) Cutler, A.; Ehnholt, D.; Giering, W. P.; Lennon, P.; Kaghn, S.; Rosan, A.; Rosenblum, M.; Tancrede, J.; Wells, D. *J. Am. Chem. Soc.* **1976**, *98*, 3495.
(9) Cotton, F. A.; Hunter, D. L. *J. Am. Chem. Soc.* **1976**, *98*, 1413.
(10) Mann, B. E. *J. Chem. Soc., Dalton Trans.* **1978**, 1761.
(11) Grassi, M.; Mann, B. E.; Spencer, C. M. *J. Chem. Soc., Chem. Commun.* **1985**, 1169.
(12) Reger, D. L.; Coleman, C. *J. Organomet. Chem.* **1977**, *131*, 153.
(13) Kreiter, C. G.; Maasbol, S.; Anet, F. A. L.; Kaez, H. D.; Winstein, S. *J. Am. Chem. Soc.* **1966**, *88*, 3444.
(14) Cotton, F. A.; Faller, J. W.; Musco, A. *J. Am. Chem. Soc.* **1968**, *90*, 1438.
(15) (a) Cotton, F. A.; Hunter, D. L.; Lahuerta, P. *J. Am. Chem. Soc.* **1974**, *96*, 7926. (b) Cotton, F. A.; Hunter, D. L.; Lahuerta, P. *J. Am. Chem. Soc.* **1974**, *96*, 4723.

0002-7863/91/1513-7513$02.50/0

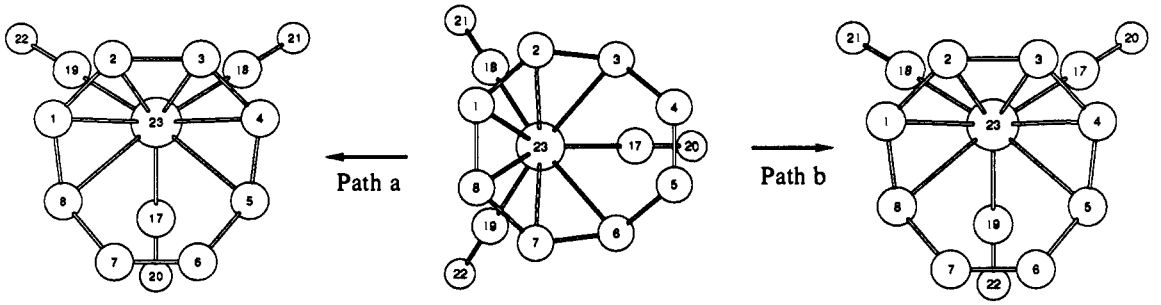

Figure 1. Two carbonyl permutations for the 1,3-shift mechanism.

The intermediate in the rearrangement process was thought to be a "piano-stool" structure in which all carbon atoms in the ring were equidistant from the metal atom, allowing equal probability for all shifts. Further evidence for the piano-stool structure was provided by the fact that (η^6-COT)(η^4-norbornadiene)Ru also rearranges by a random-shift mechanism.[16] In 1976, Whitesides and Budnik used ^{13}C NMR line-broadening analysis on the related $(C_7H_7)(CO)_3Mn$ system to conclude that rearrangement occurs via a 1,2-shift mechanism with a free energy of activation of 14 kcal/mol at 300 K.[17] They believed that the mechanism involved a 16-electron intermediate. In 1977, Mann used the Forsén–Hoffman spin-saturation method to show that $(CO)_3(\eta^6$-COT)Cr rearranges via a 1,3-shift and to a lesser extent a 1,2-shift.[18] The rates were 24 and 48 s^{-1} for the 1,2- and 1,3-shifts, respectively, at 26.5 °C. Very recently, the Gibbs free energies of activation at 298 K have been determined to be 16.2 and 15.2 kcal/mol for the 1,2- and 1,3-shifts, respectively.[19]

While the recent experimental work conclusively shows that there are two competitive shift mechanisms operative in this system, there exists no *direct* experimental evidence concerning the nature of the electronic and geometric structures of the transition states. In this paper, we present a detailed analysis of every possible shift mechanism in $(CO)_3(\eta^6$-COT)Cr. The points along the potential energy surfaces, including the estimated transition states, are generated with the linear synchronous transit (LST)/orthogonal-optimization approach[20] and the PRDDO[21] molecular orbital approximations. We will show that such an approach works beautifully on this very large and complicated system because it quickly generates potential energy surfaces without any a priori assumptions about the transition-state geometry or costly second-derivative calculations. Ab initio molecular orbital calculations are used to more accurately estimate the activation energies of the various shift mechanisms. The bonding is analyzed by dividing each molecule into $Cr(CO)_3$ and COT fragments and then considering their interaction. Localized molecular orbitals[22] (LMO) are used whenever possible to clearly define the olefin–metal bonds. We also present a method for calculating the COT to $Cr(CO)_3$ binding energy which utilizes the experimental Cr–CO bond energy of hexacarbonylchromium. The distortion energy of the COT fragment for each shift transition state is calculated in order to gauge its stability relative to the ground-state structure of COT. We show that there is a delicate interplay among the COT distortion energy, the COT to $Cr(CO)_3$ binding energy, and the overall stability of the molecule.

Computational Methods

All structures were optimized by using the PRDDO molecular orbital approximations.[21] This is a nonempirical formalism that produces relatively accurate geometries for transition-metal complexes[23] with only a modest amount of computational effort. The potential energy surfaces were obtained by using the LST/orthogonal-optimization method.[20] This procedure has worked very well in calculating many reaction pathways.[3,4,24] In this method, the path coordinate, P, is defined as

$$P = d_r/(d_r + d_p)$$

where d_r and d_p are summations of distances between identical atoms associated with an intermediate structure and the reactant and the product, respectively. They are defined as

$$d_r = [(1/N) \sum_{\omega=x,y,z} \sum_{a=1}^{N} [(\sum \omega_a(c) - \omega_a(r))^2]]^{1/2}$$

with a similar definition d_p. Here, N is the number of atoms, $\omega_a(c)$ is the x, y, or z coordinate of the current geometry, and $\omega_a(r)$ is the x, y, or z coordinate of the reactant when the reactant and product are at maximum coincidence. The reactant is usually assigned a path coordinate of 0.00 and the product a path coordinate of 1.00. Next, a continuous set of structures is generated between the product and reactant. A plot of energy versus path coordinate yields a first approximation of the potential energy surface. The geometry of the high-energy structure is then relaxed with the constraint that its path coordinate remain the same. This is called an orthogonal optimization. This procedure is repeated until the surface is adequately characterized. The highest energy structure can be viewed as an *estimate* of the transition state because the LST/orthogonal-optimization method defines a series of continuous structures and therefore the maximum-energy point on the surface is an upper bound to the true transition-state energy at the PRDDO level. A true transition state has one and only one negative eigenvalue of the Hessian matrix. In the systems examined here, calculation of the requisite second derivatives would take a prohibitively large amount of computer time. We also caution the reader that it is most unlikely that *all* of our estimated transition states correspond to stationary points with one and only one imaginary frequency. In the limited amount of geometrical space available, it is highly likely that some of our structures represent higher order transition states. Nonetheless, we shall show that our calculations are consistent with experiment in the sense that the two lowest energy pathways calculated are in fact the two pathways observed experimentally.

The structure of $(CO)_3(\eta^6$-COT)Cr was optimized in the C_s symmetry point group, starting from a combination of the X-ray crystal structure of $(CO)_3$(TMCOT)Cr[25] and the COT ring geometry in $(CO)_3$(COT)-Mo.[26] All possible d-orbital occupancies were tested in order to obtain the lowest energy configuration. All geometrical parameters were optimized except for the C–H distances and the O–C–Cr angles, which were held fixed at 1.07 Å and 180°, respectively. The PRDDO calculations were performed on a Solbourne Series 5/602 computer. A typical single-point energy calculation required about 150 s. This can be compared to 20 s on a CRAY X-MP 14/SE computer.

Once the geometry of the ground state was obtained, we proceeded to examine the potential energy surface of each shift mechanism. An obvious complication arises because in general there is more than one way

(16) Cotton, F. A.; Kolb, J. R. *J. Organomet. Chem.* **1976**, *107*, 113.
(17) Whitesides, T. H.; Budnik, R. A. *Inorg. Chem.* **1976**, *15*, 874.
(18) (a) Mann, B. E. *J. Chem. Soc., Chem. Commun.* **1977**, 626. (b) Gibson, J. A.; Mann, B. E. *J. Chem. Soc., Dalton Trans.* **1979**, 1021.
(19) Abel, E. W.; Orrell, D. G.; Qureshi, K. B.; Sik, V.; Stephenson, D. *J. Organomet. Chem.* **1988**, *353*, 337.
(20) Halgren, T. A.; Lipscomb, W. N. *Chem. Phys. Lett.* **1977**, *49*, 225.
(21) (a) Marynick, D. S.; Lipscomb, W. N. *Proc. Natl. Acad. Sci. U.S.A.* **1982**, *79*, 1341. (b) Halgren, T. A.; Lipscomb, W. N. *J. Chem. Phys.* **1973**, *58*, 1569.
(22) Boys, S. F. In *Quantum Theory of Atoms, Molecules and the Solid State*; Löwdin, P. O., Ed.; Academic Press: New York, 1966; pp 253–62.
(23) (a) Marynick, D. S.; Axe, F. U.; Kirkpatrick, C. M.; Throckmorton, L. *Chem. Phys. Lett.* **1983**, *99*, 406. (b) Marynick, D. S.; Reid, R. D. *Chem. Phys. Lett.* **1986**, *124*, 17.
(24) (a) Axe, F. U.; Marynick, D. S. *Organometallics* **1987**, *6*, 572. (b) Jolly, C. A.; Marynick, D. S. *J. Am. Chem. Soc.* **1989**, *111*, 7968. (c) Marynick, D. S.; Axe, F. U.; Hansen, L. M.; Jolly, C. A. In *Topics in Physical Organometallic Chemistry*; Gielen, M., Ed.; Freund Publishing House Ltd.: London, 1989; Vol. 3, pp 43–84.
(25) Bennett, M. J.; Cotton, F. A.; Takats, J. *J. Am. Chem. Soc.* **1968**, *90*, 903.
(26) McKechnie, J.; Paul, I. C. *J. Am. Chem. Soc.* **1966**, *88*, 5927.

to generate a given potential energy surface, depending upon which permutation of the carbonyls is chosen. For example, Figure 1 illustrates the two carbonyl permutations associated with the 1,3-shift. In most cases, this forced us to calculate two totally separate potential energy surfaces for each shift. Because the fluxional behavior results in no net change in the structure, the product and reactant have the same geometry, although the ligands are numbered differently. We started by assigning the reactant a path coordinate of 0.00 and the product a path coordinate of 1.00. Next, a continuous set of structures was generated from the reactant to the product. In the original LSTs, the 0.50 path coordinate structure was always the high-energy structure. Furthermore, the geometry conformed to C_s symmetry. Therefore, the 0.50 structures were not orthogonally optimized because the path coordinate was invariant to geometry variations within the point group of the estimated transition-state structure. Once this structure was optimized, LSTs were performed between 0.00 and 0.50. There was no need to perform LSTs from 0.50 to 1.00 because the potential energy surfaces were symmetric. LSTs and orthogonal optimizations were performed until the highest energy structure was the result of an optimization rather than a LST.

Ab initio calculations were performed on the ground-state geometry and the estimated transition-state geometry of each shift in order to more accurately determine the energetics. These calculations were performed by using the program GAMESS[27] on a CRAY X-MP 14/SE computer at the University of Texas Center for High Performance Computing (UT-CHPC) and an IBM 4381-3 computer at the University of Texas at Arlington. A typical calculation required 11 CPU hours on the IBM computer and 0.6 CPU hour on the CRAY computer. The ligands were described by a 4-31G basis set.[28] The chromium basis set was triple ζ in the 3s/3d region and double ζ in the 3p and 4sp space and included a set of 4d valence orbitals.[29] This resulted in a total of 43 contracted basis functions on the chromium atom, which gives a grand total of 185 contracted basis functions for $(CO)_3(COT)Cr$. An even larger basis set was used to further estimate the energetics for the ground state and the estimated transition states in the 1,2- and 1,3-shifts. This basis set included polarization d functions[30] on each carbon atom of the COT ring and resulted in a total of 233 contracted basis functions. Ab initio Hartree–Fock calculations with a 4-31G basis set were also performed on the COT fragments and the PRDDO-optimized COT ring.

In order to qualitatively compare the interaction between the COT ring and Cr, we added the individual Cr–C degrees of bonding[31] for the carbon ring atoms to yield a total Cr–COT degree of bonding (TDB). The COT to $Cr(CO)_3$ binding energy (BE) can also be calculated in order to more quantitatively describe this important interaction. A problem arises because the $Cr(CO)_3$ fragment is not adequately described by a single Slater determinant wave function. We therefore prefer to estimate the BE with the following thermodynamic cycle:

$$Cr(CO)_6 + COT \rightarrow (CO)_3(COT)Cr + 3CO \quad \Delta E_1 \qquad (1)$$

$$3CO + Cr(CO)_3 \rightarrow Cr(CO)_6 \quad \Delta E_2 \qquad (2)$$

$$\text{net:} \quad Cr(CO)_3 + COT \rightarrow (CO)_3(COT)Cr \quad BE \qquad (3)$$

ΔE_1 for reaction 1 can be readily calculated at the ab initio Hartree–Fock level using PRDDO-optimized geometries. ΔE_2 can be estimated from the experimentally determined average bond-dissociation energy of hexacarbonylchromium, −29.5 kcal/mol.[32] The BE is now easily obtained as the sum of ΔE_1 and ΔE_2. This procedure avoids the necessity of using a multiple configurational wave function to describe the $Cr(CO)_3$ fragment. Our approach yields an estimated COT to $Cr(CO)_3$ binding energy of about 40 kcal/mol, which seems somewhat low considering the typical olefin binding energies for first-row metals are ~20 kcal/mol per bond; however, it must be remembered that the COT ligand must distort significantly to bind to the metal in an η^6 fashion, and this will tend to lower the overall BE. By themselves, the BEs are directly related to the relative energies of the various transition-state structures. A more useful quantity can be extracted by breaking reaction 3 into two parts. These additional steps are shown as reactions 4 and 5. In reaction 4, the COT ring is distorted into its geometry in the chromium complex. ΔE_3 is calculated at the ab initio Hartree–Fock level. This allows calculation of the energy of binding of the *distorted* COT fragment to $Cr(CO)_3$ by simply subtracting ΔE_3 from BE. This quantity will be denoted BE′ in order to avoid confusing it with BE, the binding energy of COT.

$$COT \rightarrow COT_{distorted} \quad \Delta E_3 \qquad (4)$$

$$COT_{distorted} + Cr(CO)_3 \rightarrow (CO)_3(COT)Cr \quad BE' \qquad (5)$$

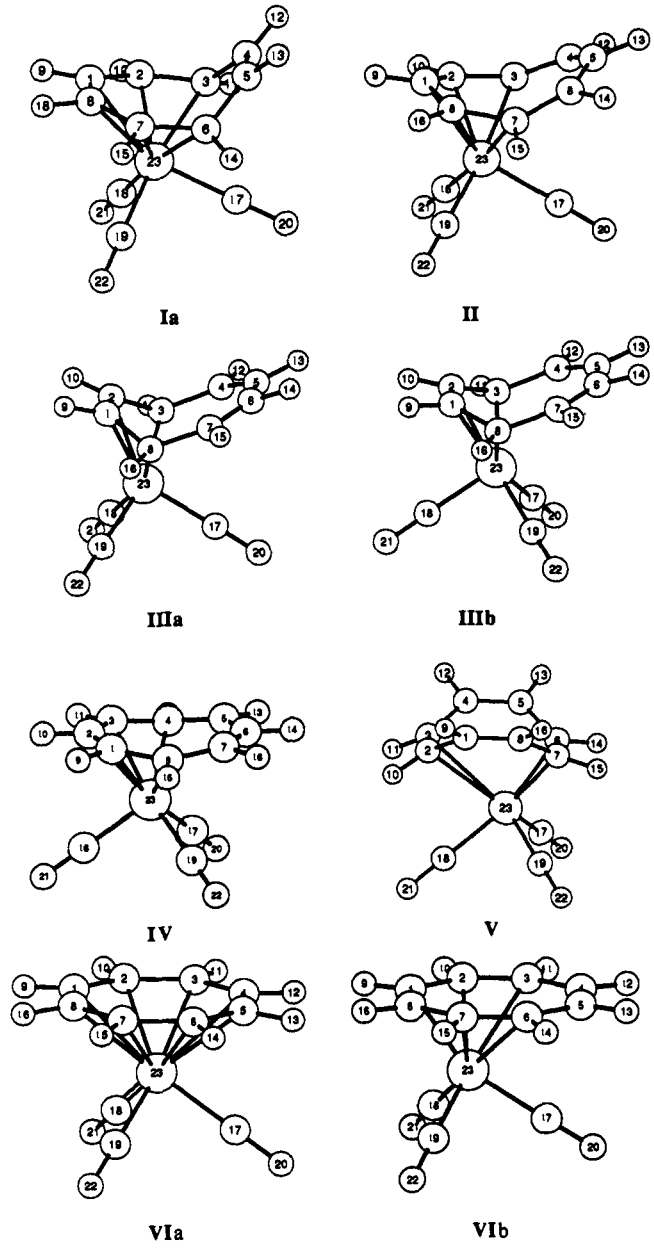

Figure 2. Ground-state geometry (Ia) and estimated transition states in the 1,2-shift (II), the 1,3-shift (IIIa is path a and IIIb is path b), the 1,4-shift (IV), and the 1,5-shift (V). The "piano-stool" structure is shown as VIa, and the distorted "piano-stool" structure, as VIb.

Results and Discussion

Ground-State Structure. In order for any molecular orbital calculation to be useful, the method must be able to reasonably represent the structure of the molecule being studied. To our

(27) Schmidt, M. W.; Boatz, J. A.; Baldridge, K. K.; Koseki, S.; Gordon, M. S.; Elbert, S. T.; Lam, B. *QCPE Bull.* **1987**, *7*, 115.

(28) Ditchfield, R.; Hehre, W. J.; Pople, J. A. *J. Chem. Phys.* **1970**, *54*, 724.

(29) This is basis set A for the ^5D atomic configuration of chromium in: Hansen, L. M.; Marynick, D. S. *J. Phys. Chem.* **1988**, *92*, 4588. These basis sets are designed to utilize the sixth Cartesian Gaussian d function to describe the 3s orbital on the metal. Each basis function is a Gaussian expansion of a Slater type orbital (STO). The 1s, 2s, and 2p orbitals are described by a three-Gaussian (3G) expansion of single-ζ-STOs with exponents of 23.408, 8.494, and 10.040, respectively. The 3p and 4sp orbitals are described by a two-term Gaussian expansion of a double-ζ-STO. The exponents are 4.6 and 2.858 for the 3p and 2.3 and 1.27 for the 4sp shell. The 3d orbital is a 2G expansion of a triple-ζ-STO with orbital exponents 8.588, 4.203, and 1.997. A valence 4d basis function that consisted of a 1G expansion of a STO with an orbital exponent of 2.0 was also used.

(30) The d functions consisted of a 1G expansion of a STO whose orbital exponent was 0.75.

(31) The degrees of bonding are 1 for a single bond, 2 for a double bond, etc.

(32) Skinner, H. A. In *Advances in Organometallic Chemistry*; Stone, F. G. A., West, R., Eds.; Academic Press: New York, 1964; Vol. 2, p 49.

Table I. Geometrical Parameters for Ia, Ib, $(CO)_3(COT)Mo$,[a] and $(CO)_3(TMCOT)Cr$[b]

Distances, Å

	R(M–X)			
X	Ia	Ib	$(CO)_3(COT)Mo$	$(CO)_3(TMCOT)Cr$
C^1	2.17	2.21	2.34	2.23
C^2	2.15	2.19	2.29	2.20
C^3	2.20	2.12	2.47	2.29
C^4	2.96	2.99	3.24	3.15
C^5	2.96	2.99	3.24	3.16
C^6	2.20	2.12	2.47	2.41
C^7	2.15	2.19	2.29	2.21
C^8	2.17	2.21	2.34	2.25
C^{17}	1.92	1.97	2.00	1.86
C^{18}	1.92	1.91	1.98	1.84
C^{19}	1.92	1.91	1.98	1.85

	R(C–C)			
C–C	Ia	Ib	$(CO)_3(COT)Mo$	$(CO)_3(TMCOT)Cr$
C^1–C^2	1.39	1.36	1.39	1.42
C^2–C^3	1.37	1.43	1.38	1.40
C^3–C^4	1.47	1.49	1.49	1.48
C^4–C^5	1.30	1.30	1.27	1.30
C^5–C^6	1.47	1.49	1.49	1.48
C^6–C^7	1.37	1.43	1.38	1.39
C^7–C^8	1.39	1.36	1.39	1.44
C^8–C^1	1.38	1.44	1.44	1.40

	R(C–O)			
C–O	Ia	Ib	$(CO)_3(COT)Mo$	$(CO)_3(TMCOT)Cr$
C^{17}–O^{20}	1.15	1.15	1.12	1.15
C^{18}–O^{21}	1.15	1.15	1.16	1.16
C^{19}–O^{22}	1.15	1.15	1.16	1.16

Angles, deg

	Ia	Ib	$(CO)_3(COT)Mo$	$(CO)_3(TMCOT)Cr$
C^{17}–Cr–C^{18}	91	88	92	91
C^{17}–Cr–C^{19}	91	88	92	94
C^{18}–Cr–C^{19}	88	88	79	81
$C^{1,8}$–$C^{2,7}$–$C^{3,6}$[d]	173	174		
$C^{2,7}$–$C^{3,6}$–$C^{4,5}$	128	117	130[c]	119[c]

[a] Reference 26. [b] Reference 25. [c] Best plane through atoms 1, 2, 3, 6, 7, and 8 and atoms 3, 4, 5, and 6. [d] The notation $C^{1,8}$–$C^{2,7}$–$C^{3,6}$ refers to the angle between the midpoints of atoms 1/8, 2/7, and 3/6.

knowledge, no X-ray crystal structure of $(CO)_3(\eta^6\text{-COT})Cr$ exists in the literature, but structures of similar compounds do exist. For example, the X-ray crystal structures of $(CO)_3(\eta^6\text{-TMCOT})Cr$[25] and $(CO)_3(\eta^6\text{-COT})Mo$[26] each contain an η^6-C_8 fragment. For comparison, we present structural parameters for the PRDDO ground-state geometry of $(CO)_3(\eta^6\text{-COT})Cr$ (Ia), $(CO)_3(\eta^6\text{-TMCOT})Cr$, and $(CO)_3(\eta^6\text{-COT})Mo$ in Table I. The numbering system used is shown in Figure 2. The average C–C internuclear distance for the six carbon atoms coordinated to the metal is 1.40 Å in $(CO)_3(COT)Mo$ and 1.41 Å in $(CO)_3(TMCOT)Cr$. The C^4–C^5 distance is 1.27 Å in the molybdenum complex and 1.30 Å in $(CO)_3(TMCOT)Cr$. The C^3–C^4 and C^5–C^6 bonds have single-bond lengths of about 1.5 Å in both structures. Another feature of the ring is the angle made by the intersection of the two planes defined by atoms 1, 2, 3, 6, 7, and 8 and atoms 3, 4, 5, and 6. This angle is 119° in $(CO)_3(TMCOT)Cr$ and 130° in $(CO)_3(COT)Mo$. Examining Table I, one can see that the PRDDO-optimized COT ring geometry is in good agreement with experiment. The average C–C internuclear distance for carbon atoms attached to chromium is 1.38 Å. The C^4–C^5 internuclear distance is 1.30 Å. The C^3–C^4 bond length and its symmetry-equivalent C^5–C^6 bond length are 1.47 Å. The angle between the two planes defined above is 128°. It is comforting to see that this value is much closer to the angle in the molybdenum complex because, as noted in the Introduction, $(CO)_3(COT)M$ molecules rearrange by a 1,3-shift mechanism whereas $(CO)_3(TMCOT)M$ molecules rearrange via a 1,2-shift mechanism. The average Cr–C distance for the olefinic carbon atoms attached to Cr is 2.26 Å in $(CO)_3(TMCOT)Cr$, compared to 2.17 Å for the optimized structure of the parent compound. While our optimized Cr–C distances appear to be somewhat short, it is clear from Table I that direct comparisons are difficult due to the asymmetry induced by the methyl substituents in $(CO)_3(TMCOT)Cr$ (compare for example the Cr–C^3 and Cr–C^6 distances, which are symmetry equivalent in the parent system but differ by 0.13 Å in the crystal structure of $(CO)_3(TMCOT)Cr$). Thus, it is important to examine Cr–C distances in other related compounds. The average $Cr–C_{ring}$ distances are 2.24, 2.27, 2.15, and 2.21 Å in tricarbonyl(naphthalene)chromium(0),[33] tricarbonyl(cyclooctatrienyl)chromium(0),[34] bis(benzene)chromium(0),[35] and (benzene)tricarbonylchromium(0),[36] respectively. Thus, the PRDDO-optimized values in Table I fit well into the range of Cr–C distances stated above. The Cr–CO distances are all 1.92 Å in the PRDDO-optimized geometry of $(CO)_3(\eta^6\text{-COT})Cr$, which is in reasonable agreement with that found in $(TMCOT)Cr(CO)_3$. For comparison, the chromium–carbonyl distance in the PRDDO-optimized geometry of $Cr(CO)_6$ is 1.90 Å, which is in excellent agreement with the experimental value of 1.91 Å.[37] Overall, the PRDDO-optimized geometry is in good agreement with available experimental data.

Having described the geometry of the ground-state molecule, we now turn to the electronic factors involved in stabilizing the molecule. This is best accomplished by dividing the molecule into an olefin fragment and a metal tricarbonyl fragment. The interaction between these two fragments will involve charge donation from the COT to the unoccupied chromium orbitals (forward bonding) and electron donation from the metal to the olefin virtual orbitals (back-bonding). Cyclooctatetraene is an eight-π-electron system. It is a "tub"-shaped,[38] nonaromatic molecule because is does not abide by the $4n + 2$ Hückel rule. In $(CO)_3(\eta^6\text{-COT})Cr$, the ring flattens out so that six of the eight carbon atoms are contained in a single plane. This requires 33 kcal/mol of energy. The consequences of the ring flattening are 2-fold. First, three instead of only two of the double bonds in the COT ring may now donate charge to the tricarbonyl fragment. Second, this flattening lowers the energy of the lowest unoccupied molecular orbital (LUMO) so that it can more readily accept electrons from the $Cr(CO)_3$ fragment. The nodal character of the three occupied molecular orbitals (MOs) and the LUMO of the COT portion that interacts with Cr are as shown in diagram **1**. The molecular

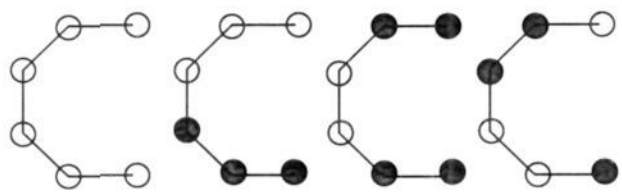

1

orbitals of the tricarbonyl fragments are generated by removing three *fac* carbonyls from hexacarbonylchromium.[39] The t_{2g} orbitals of the original hexacarbonylchromium are stabilized by interactions with the carbonyls but are still available for back-bonding with the olefin. The $e_g + a_1$ orbitals in the $Cr(CO)_3$ fragment are reduced to $2a' + a''$ in C_s symmetry. Their localized representation can be depicted as shown in **2**. In a symmetry basis, these orbitals are of the correct symmetry to accept electrons from the occupied 1a', 1a", and 2a' orbitals of the COT fragment shown in **1**. Thus, a strong interaction between Cr and COT is formed. A detailed molecular orbital analysis indicates that this is the most important contribution to the binding energy of the

(33) Kunz, V.; Nowacki, W. *Helv. Chim. Acta* **1967**, *50*, 1052.
(34) Armstrong, V. S.; Prout, C. K. *J. Chem. Soc.* **1962**, 3770.
(35) Kuelen, E.; Jellinek, F. *J. Organomet. Chem.* **1966**, *5*, 490.
(36) Chiu, N.; Schafer, L.; Seip, R. *J. Organomet. Chem.* **1975**, *101*, 331.
(37) Rees, B.; Mitschler, A. *J. Am. Chem. Soc.* **1976**, *98*, 7918.
(38) Claus, K. H.; Kruger, C. *Acta Crystallogr.* **1988**, *C44*, 1632.
(39) Elian, M.; Hoffmann, R. *Inorg. Chem.* **1975**, *14*, 1058.

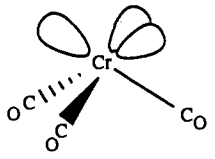

2

two fragments. If we drastically reduce the back-bonding capability of the metal tricarbonyl fragment by substituting Fe^{2+} for Cr in Ia then an LMO analysis places double bonds between the following atoms: C^2–C^3, C^4–C^5, C^6–C^7, C^8–C^1. Thus, the double bonds in the ring are clearly oriented toward the 2a′ + a″ frontier orbitals of the tricarbonyl fragment. Furthermore, if we connect the midpoints of the double bonds to the metal, then it becomes clear that the metal is in a quasi-octahedral environment.

The forward bonding is the most important contribution to the bonding of the two fragments, but there is also a stabilizing effect due to back-bonding. This is apparent in the molecular orbital just below the HOMO of $(CO)_3(\eta^6\text{-COT})Cr$, where an admixture of one of the t_{2g} orbitals of the original hexacarbonylchromium and the LUMO of the COT fragment is found. Therefore, this MO represents charge transfer from chromium to a π antibonding orbital on cyclooctatetraene. We first confirmed a strong back-bonding interaction when *four* LMOs were obtained between chromium and the ring. The extra LMO is due to back-bonding, which is so strong that, in effect, it is represented as a three-center bond in the localized basis. A similar case was found in (butadiene)tricarbonyliron,[40] where two localized molecular orbitals were expected but three were actually obtained. In conclusion, forward bonding dominates the interaction between COT and $Cr(CO)_3$ but there is also a significant stabilizing contribution due to back-bonding.

We shall see that the fluxional behavior of $(CO)_3(COT)Cr$ is intimately tied to the orientation of the $Cr(CO)_3$ unit. Therefore, it is advantageous to examine the conformation of the $(CO)_3(\eta^6\text{-COT})Cr$ molecule obtained by rotating the $Cr(CO)_3$ unit 180° and reoptimizing the geometry. This structure has the unique carbonyl pointing away from the center of the COT ring. The structure that results is shown in the diagram for Ib. Ib is 12.9

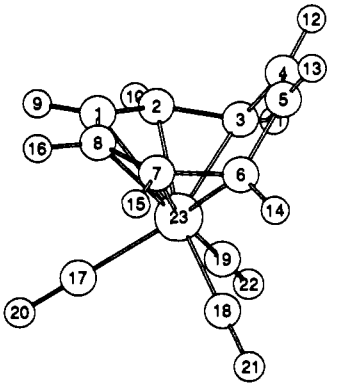

Ib

kcal/mol higher in energy than Ia at the ab initio Hartree–Fock level of theory. This is very close to the Gibbs free energy of activation of 11.6 kcal/mol required to scramble nonequivalent carbonyls in $(CO)_3(COT)Cr$.[41] There are several important geometrical changes that occur when the unique carbonyl is pointed away from the interior of the ring. For example, the C–C bond lengths of the carbon atoms bonded to Cr change considerably. Neglecting symmetry equivalent distances, $R(C^8\text{–}C^1)$, $R(C^1\text{–}C^2)$, and $R(C^2\text{–}C^3)$ become 1.44, 1.36, and 1.43 Å, respectively, in Ib compared to 1.38, 1.39, and 1.37 Å in Ia. Another significant difference is the angle formed by the two planes defined by atoms 1, 2, 3, 6, 7, and 8 and atoms 3, 4, 5, and 6. For the low-energy structure this angle is 128°, but for the high-energy conformation this angle is 117°.

The rotation of the $Cr(CO)_3$ unit orients its unoccupied 2a′ + a″ molecular orbitals, shown previously, in a fashion such that they no longer protrude toward the quasi-double bonds of the COT fragment. This is the major destabilizing factor. It can be seen most clearly by again reducing the back-bonding effects via substitution of Fe^{2+} for Cr^0. The ΔE between Ib and Ia, at the PRDDO level, increases from 16.2 to 32.3 kcal/mol when the metal is changed from Cr^0 to Fe^{2+}. Thus, if Ia and Ib must rely only on forward bonding, then Ib becomes even more destabilized compared to Ia. In the iron analogue, the localized orbitals of Ib clearly correspond to a trigonal-prism environment, and indeed the calculated ΔE of ~32 kcal/mol is of the same order as has been found computationally for the octahedral/trigonal-prismatic energy difference in d^6 complexes such as $(CO)_5(PH_3)Cr$.[3] Although there is a definite decrease in forward bonding in Ib, the back-bonding seems to have increased compared to that in Ia. This must be the case, because the BE′ is larger in Ib than in Ia by 15 kcal/mol (see Table III). This indicates that the Cr–COT interaction has increased. However, there is a substantial energy payment for the increase in Cr–COT bonding that is manifested in the 60.5 kcal/mol required to deform COT into its geometry in Ib. This is almost 30 kcal/mol more than is required to distort the COT ring in Ia. The BE′ is not large enough to offset this distortion energy, thus making Ib overall less stable than Ia.

In conclusion, we see that changing the chromium atom's environment from octahedral to trigonal prismatic costs a total of ~13 kcal/mol. This is partially due to a smaller amount of forward bonding because the unoccupied orbitals of the tricarbonylchromium fragment are no longer oriented in such a way that they can readily accept electrons from the π orbitals of the COT ring. We also see the delicate interplay between the strength of the Cr–COT interaction and the destabilization of the COT ring. The Cr–COT bonding is stronger in the less stable structure, but this is offset by a larger COT destabilization energy. These act in opposing directions, and in this case, the destabilization of the ring outweighs the metal–ring stabilization. Thus, Ia is more stable than Ib.

The Ring-Shift Mechanisms. Having elucidated the electronic and geometric structure of the ground state, we now focus our attention on the various ring-shift mechanisms. As alluded to previously, a problem arises with respect to the permutation of the carbonyls because in all shift mechanisms there are two possible rotations of the carbonyls. This is illustrated for the 1,3-shift by paths a and b in Figure 1. In path a, the carbonyl in the symmetry planes of the reactant and product is the same, whereas in path b the carbonyl in the symmetry plane changes upon going from reactant to product. These two pathways will result in transition-state geometries, which differ by a 60° rotation of the carbonyls. In order to completely investigate the shift mechanisms, we performed LST/orthogonal optimizations for both permutations of the carbonyls in all pathways except for the one involving the piano-stool structure. In every mechanism studied, the low-energy pathway was the one that resulted in the least motion of the carbonyls. This is a significant finding and will be discussed later. The products that result from the lowest energy pathway of each shift are shown in Scheme I.

The ΔE's for each transition state, at the ab initio level of calculation, are contained in Table II. The calculated activation barriers are too low when compared to experimental data, but they increase in the shift order 1,3 < 1,2 < 1,4 < 1,5 < random, consistent with the experimental findings. We will first discuss the ring-shift mechanisms that produce large activation energies, i.e. the random-shift, the 1,4-shift, and the 1,5-shift, before discussing the details of the two lowest energy shift pathways.

The Random-Shift Mechanism. The piano-stool structure has been used to describe many organometallic structures in which a cyclic olefin is bonded to a metal carbonyl moiety. Examples can be seen throughout the transition metals, e.g. $(\eta^6\text{-}C_6H_6)$-

(40) Marynick, D. S.; Kirkpatrick, C. M. *THEOCHEM* **1988**, *169*, 245.
(41) Kreiter, C. G.; Lang, M.; Strack, H. *Chem. Ber.* **1975**, *108*, 1502.

Table II. Relative Energies (kcal/mol)[a]

	ΔE	ΔE^b
Ib	+12.9	
1,2-shift (II)	+6.3	+8.9
1,3-shift (path a, IIIa)	+23.8	
1,3-shift (path b, IIIb)	+0.6	+2.9
1,4-shift (IV)	+10.0	
1,5-shift (V)	+11.6	
piano stool (VIa)	+17.6	
distorted piano stool (VIb)	+5.4	

[a] At the ab initio Hartree–Fock level of calculation. The relative energies at the PRDDO level are 16.2, 28.1, 15.5, 8.3, 39.5, 29.1, 50.3, and 29.2 kcal/mol for Ib, II, IIIa, IIIb, IV, V, VIa, and VIb, respectively. [b] Diffuse d function on carbon atoms of ring (ζ = 0.75).

Table III. COT to $Cr(CO)_3$ Binding Energy (BE), Energy Required To Distort COT (ΔE_3), and Energy for Binding of the Distorted COT Fragment to $Cr(CO)_3$ (BE′) for the Ground State and Various-Shift Transition States (kcal/mol)

	BE	ΔE_3	BE′
Ia	−40.1	+32.9	−73.0
Ib	−27.3	+60.5	−87.8
1,2-shift (II)	−33.8	+48.2	−82.0
1,3-shift (path a, IIIa)	−16.3	+86.3	−102.6
1,3-shift (path b, IIIb)	−39.5	+52.4	−91.9
1,4-shift (IV)	−30.2	+43.8	−74.0
1,5-shift (V)	−28.5	+11.9	−40.4
piano stool (VIa)	−22.5	+35.8	−58.3
distorted piano stool (VIb)	−34.8	+19.8	−54.6

$(CO)_3Cr$, $(CO)_3(\eta^5\text{-}C_5H_5)Mn$, $(CO)_3(\eta^4\text{-}C_4H_4)Fe$, etc. Therefore, there is a reasonable possibility that the fluxional behavior of $(CO)_3(COT)Cr$ occurs via a similar structure. This was Cotton's conjecture when his experimental results indicated that either a 1,3-shift or a random shift was occurring.[15] We chose to optimize two piano-stool structures. One uses a strict definition by requiring all R(C–C) and R(Cr–C) distances to be equal. The other one we shall denote as a distorted piano stool because the C–C and Cr–C bond lengths were relaxed although the ring was still required to be planar.

The structure with C_{8v} symmetry in the COT ring and all R(Cr–C) distances equal is shown as VIa in Figure 2. This structure has equal probability of relaxing to any shift product. Its energy is 17.6 kcal/mol higher than that of the ground-state structure, as seen in Table II. The PRDDO optimization produces chromium–ring carbon distances of 2.37 Å. All C–C distances in the ring are 1.39 Å, and the hydrogen atoms bend downward 3.8° from the carbon ring plane. If all four electron pairs in the ring are interacting with chromium, then, in a formal sense, the COT ring donates eight electrons to the total electron count. In this scenario, VIa is a 20-electron complex. However, the LMO description produces four C–C double bonds with an average delocalization to the Cr of ~0.06e. This indicates that there is very little forward bonding. Furthermore, there is only one chromium–ring LMO corresponding to Cr to COT back-bonding. It consists of 0.8e on Cr and ~0.1e on each of the ring carbon atoms and is actually a *nine*-center orbital! This leads to a small BE′ of −58.3 kcal/mol, shown in Table III, and a TDB of 1.75. The existence of only one LMO in the Cr–COT region of the molecule is consistent with the weak orbital overlap and relatively high energy of this structure.

The distorted piano-stool structure that was optimized in C_s symmetry is shown as structure VIb in Figure 2. It lies only +5.4 kcal/mol higher in energy than the ground-state structure. The $Cr(CO)_3$ fragment moves to one side of the ring so as to increase Cr–COT orbital overlap. Thus, the R(Cr–C) distances become asymmetric and vary from 2.12 to 2.91 Å.

Compared to that of the ground state, the Cr–COT bonding is decreased. This is seen by the TDB and BE′, which are 0.54 and 18.4 kcal/mol smaller, respectively, in VIb. This difference is mostly due to the loss of interaction between the metal and C^3 and C^6. For the ground-state structure, the Cr–C^3 and Cr–C^6 degrees of bonding are 0.49 compared to 0.22 in VIb. This is clearly related to the increased distance for Cr–C^3 and Cr–C^6 in VIb relative to Ia (see Tables I and IV). Although the Cr–COT bonding is ~18 kcal/mol weaker in VIb than in the ground state (compare BE′ values in Table III), its overall ΔE is only 5.4 kcal/mol because the COT distortion energy is 13 kcal/mol less. Again, we see the interplay between the COT distortion energy and Cr–COT bond strength. In this case, the Cr–COT bonding interaction is weaker but this is compensated by a lower COT distortion energy. Although VIb is relatively low in energy, it *cannot* be a common intermediate through which all shifts would proceed. This structure will produce different transition states for each shift because Cr is asymmetrically situated with respect to its distances from the carbon ring atoms. As we will see below, this structure is not a saddle point but represents a point on or

Table IV. Geometric Parameters for the Estimated Transition States[a]

	R(Cr–X), Å						
X	1,2-shift, II	1,3-shift, path a, IIIa	1,3-shift, path b, IIIb	1,4-shift, IV	1,5-shift, V	piano stool, VIa	distorted piano stool, VIb
C^1	2.15	2.12	2.12	2.21	2.94	2.37	2.12
C^2	2.07	2.12	2.12	2.12	2.57	2.37	2.29
C^3	2.29	2.01	2.08	2.21	2.57	2.37	2.57
C^4	2.99	2.97	2.87	2.32	2.94	2.37	2.91
C^5	3.34	3.47	3.28	2.66	2.77	2.37	2.91
C^6	2.99	3.47	3.28	2.73	2.07	2.37	2.57
C^7	2.29	2.97	2.87	2.66	2.07	2.37	2.29
C^8	2.07	2.01	2.08	2.32	2.77	2.37	2.12
C^{17}	1.98	1.91	1.94	1.99	1.90	1.96	1.95
C^{18}	1.93	1.95	1.92	1.93	1.96	1.96	1.92
C^{19}	1.93	1.95	1.94	1.99	1.90	1.96	1.92
	R(C–C), Å						
C–C	1,2-shift, II	1,3-shift, path a, IIIa	1,3-shift, path b, IIIb	1,4-shift, IV	1,5-shift, V	piano stool, VIa	distorted piano stool, VIb
C^1–C^2	1.38	1.35	1.38	1.38	1.43	1.39	1.45
C^2–C^3	1.43	1.45	1.41	1.38	1.35	1.39	1.32
C^3–C^4	1.38	1.48	1.47	1.38	1.46	1.39	1.45
C^4–C^5	1.37	1.31	1.32	1.39	1.32	1.39	1.31
C^5–C^6	1.37	1.46	1.46	1.38	1.45	1.39	1.45
C^6–C^7	1.38	1.31	1.32	1.38	1.35	1.39	1.39
C^7–C^8	1.43	1.48	1.47	1.39	1.43	1.39	1.45
C^8–C^1	1.38	1.45	1.41	1.38	1.36	1.39	1.31

Scheme I. The Product Associated with the Low-Energy Pathway of Each Shift Mechanism

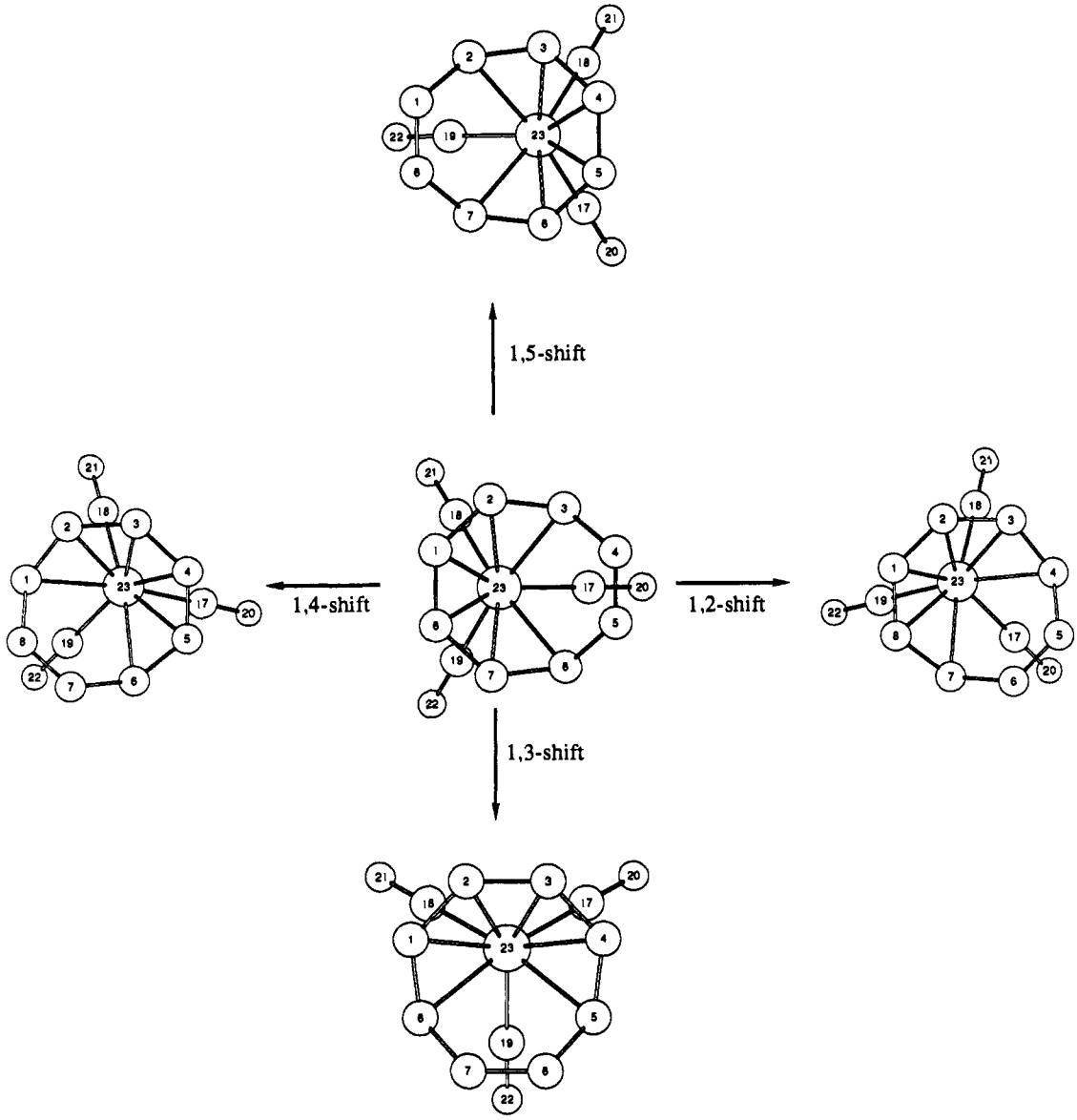

near the 1,4-shift potential energy surface.

The 1,5-Shift Mechanism. The 1,5-shift requires the longest journey by the $Cr(CO)_3$ fragment. The $Cr-C^1$ and $Cr-C^8$ bonds must be cleaved and replaced by $Cr-C^4$ and $Cr-C^5$ bonds. This produces an interesting transition state shown as structure V in Figure 2. Its energy is 11.6 kcal/mol above the ground state. At first glance, the structure resembles a 1-2:5-6-η-COT-bonded species. However, this is deceiving. The chromium atom is much closer to C^6 and C^7 than it is to C^2 and C^3 (these bond lengths are 2.07 and 2.57 Å, respectively). Therefore, although the $Cr(CO)_3$ unit traverses the ring, it does so by traveling along the *border* of the ring. The C^6 and C^7 interaction with Cr is quite large, but there is very little bonding between chromium and C^2 and C^3. This can be clearly seen in the degrees of bonding of the olefin with chromium. The degrees of bonding (DOBs) for the $Cr-C^6$ and $Cr-C^7$ bonds are each 0.57. Together they contribute more than three-quarters to the TDB of 1.57. Thus, the 1,5-shift transition state is really a 14-electron complex because the COT ring donates only one electron pair. A compensating factor is the COT distortion energy, which is by far the lowest of any structure, including the ground state. We note that a larger metal atom might be able to "straddle" the COT ring and bond in an η^4 fashion. This is most likely why ring whizzing in Os(η^6-COT)(COD) occurs via a 1,5-shift.[11]

The 1,4-Shift Mechanism. If the LST/orthogonal-optimization method is used for the 1,4-shift, then the following transition-state geometry is produced:

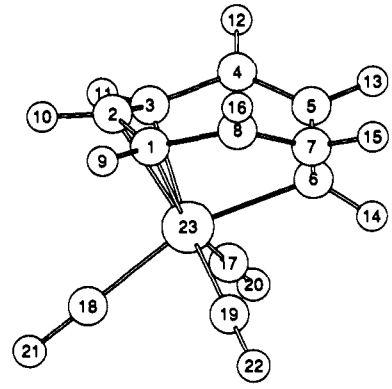

This structure lies 25.4 kcal/mol higher in energy than Ia. The transition state reflects the fact that during the reaction the $Cr-C^7$ and $Cr-C^8$ bonds are broken and the $Cr-C^4$ and $Cr-C^5$ bonds are formed. Thus, the $R(Cr-C^7)$ and $R(Cr-C^8)$ distances are increasing and the $R(Cr-C^4)$ and $R(Cr-C^5)$ distances are decreasing as the shift proceeds from reactant to product. This produces the extremely contorted COT ring shown. The COT distortion energy

(ΔE_3) is 113 kcal/mol! While the distortion energy is clearly overestimated because a noncoordinated COT with this structure would have significant biradical character, the overall energy of the structure is clearly dominated by the distortion energy of the ligand.

The 1,4-shift can actually proceed with a lower activation energy because there is an alternate pathway available that involves the distorted piano-stool structure, VIb. If one assumes that VIb is on or "near" the surface of the 1,4-shift, then it is possible to map out a new surface by defining LSTs from Ia to VIb and from VIb to the 1,4-shift product. While the LST from Ia to VIb is straight uphill energetically, a transition state (structure IV, Figure 2) can be isolated through LSTs from VIb to its 1,4-shift product. The ΔE of this new transition-state structure is 10.0 kcal/mol. Thus, the original LST approximation of the 1,4-shift transition state is not realistic enough to converge to IV directly. It is also worth noting that if one assumes that VIb is on or near the surface for the 1,2- and 1,5-shift reactions and uses it as an intermediate point in their reactions, then transition states that correspond exactly to II and V are obtained.

The 1,4-shift transition state, IV, is characterized by the following geometry. The R(Cr–C), for the five carbon ring atoms attached to Cr, range from 2.12 to 2.32 Å. The C–C bond lengths in the ring are 1.38–1.30 Å. Thus, it appears that the double bonds are completely delocalized throughout the ring. The TDB is 1.89, which indicates that the ring is not strongly bound to $Cr(CO)_3$; however, the energy required to distort the COT ring to its geometry in IV is only 44 kcal/mol. Thus, the COT ring is much less contorted than the COT ring from the original LSTs. In summary, the 1,4-shift can proceed through a transition state that contains a relatively planar η^5-COT ring.

The 1,2-Shift Mechanism. The 1,2-shift requires the least amount of motion by chromium, with only one chromium–ring carbon bond being broken or formed. The estimated transition-state geometry is shown as structure II in Figure 2. Its energy is only 6.3 kcal/mol above the ground state, Ia, and 8.9 kcal/mol higher with polarization d functions on the carbon ring atoms. The small amount of motion by chromium is consistent with the fact that this type of shift is the most common one found in cyclic olefins.[1] During the course of the reaction, the double bond between atoms C^4 and C^5 is transformed into a single bond; i.e. the C^4–C^5 bond length must increase from 1.30 to 1.47 Å. Furthermore, the bond between Cr and C^6 is cleaved and a bond is formed between Cr and C^4. The estimated transition state reflects both of these transformations. The C^4–C^5 bond length is 1.37 Å, which is a little less than halfway to its length in the product. C^4 and C^6 become symmetry equivalent and are ~3 Å from chromium. There is a plane of symmetry through C^1, C^5, C^{17}, O^{20}, and Cr. This causes some awkward geometric constraints because it is not possible for the ring to assume an alternate single-bond/double-bond arrangement. Thus, the ring is unable to localize any of the double bonds. This is reflected by the C–C bond distances, which are all equal to 1.40 ± 0.03 Å in II. The conformation of the ring is such that five carbons interact significantly with chromium. The R(Cr–C) bond lengths vary from 2.07 to 2.29 Å.

As alluded to above, the plane of symmetry that is defined by atoms 1, 5, 13, 17, 20, and 23 precludes a localized valence description that contains alternating single and double bonds. Nevertheless, the calculated Boys LMOs are still useful to obtain a qualitative feeling for the metal–olefin bonding. The LMOs reflect the C_s symmetry of the molecule. We find a three-center C^1–C^2–Cr (and symmetry-equivalent C^1–C^8–Cr) LMO, with electron populations of 0.51e, 1.02e and 0.40e, respectively. Thus, the bonding in this region of the molecule is quite reminiscent of that found in bis(allyl)nickel.[40] Only one LMO is found between the C^2–C^3 and C^7–C^8 atom pairs. Thus, these bonds are best classified as single bonds. This is also borne out in their degree of bonding, which is 1.09. The C^3–C^4 and C^6–C^7 LMOs are heavily skewed toward the C^3 and C^6, respectively. This enables them to donate a small amount of charge to Cr. The electron populations are 1.24e (C^3), 0.49e (C^4), and 0.17e (Cr) for this LMO. Finally, a three-center C^4–C^5–C^6 LMO (with population of 0.39e, 1.18e, and 0.39e, respectively) is found. The existence of five olefin LMOs excluding the σ framework, as previously found for the ground-state structure, clearly points to the importance of back-bonding in this structure. Indeed, the BE′ for COT in this structure is larger than that of the ground state, but this effect is offset by the larger olefin distortion energy (see Table III). We tend to think of the main bonding interaction here as an allylic fragment (C^8, C^1, and C^2) binding to Cr. There is also a smaller bonding contribution due to the delocalization of the C^3–C^4 and C^6–C^7 double bonds toward chromium.

The transition state discussed above is due to a least-motion pathway of the carbonyls. There are systems for which the shift mechanism involves scrambling of the carbonyls and thus a *non-least*-motion pathway. For example, it has been shown that the ring-whizzing mechanism in $Fe(\eta^4\text{-COT})(CO)_2(CNPr^i)$ does not occur by a least-motion pathway of the $Fe(CO)_2(CNPr^i)$ unit.[42] The difference between the two permutations results in a 60° rotation of the $M(CO)_2L$ unit in the transition state. These are represented as structures A and B in **3**. In the d^8 $Fe(\eta^4$-COT$)(CO)_2(CNPr^i)$ system, B is lower in energy than A. However, for our d^6 Cr system the opposite is true. The alert reader will already have deduced that a non-least-motion 1,2-shift will pass through a structure that is geometrically identical with the 1,4-shift transition-state geometry (structure IV in Figure 2). Thus, the non-least-motion 1,2-shift has an activation energy of 10.0 kcal/mol. Although the difference in energy between these two pathways is small, our calculations suggest that the mechanism probably does not permute inequivalent carbonyls. There is some indirect evidence to support the calculated preference for a least-motion 1,2-shift. For example, if the 1,2-shift occurred via a non-least-motion pathway, which has a transition-state structure geometrically identical with the least-motion 1,4-shift, then we would expect to see a competition between these two shift mechanisms. Experimentally, a 1,4-shift is not observed, and therefore the occurrence of a non-least-motion 1,2-shift seems unlikely.

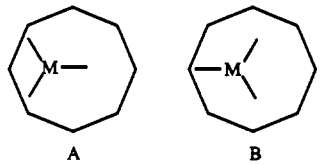

3

The 1,3-Shift Mechanism. In the 1,3-shift, the double bond migrates from atoms 4 and 5 to atoms 6 and 7 while the bonds to chromium change from atoms 1, 2, 3, 6, 7, and 8 to atoms 1, 2, 3, 4, 5, and 8. The two carbonyl permutations in Figure 1 produce different transition-state structures, which are shown in Figure 2 as IIIa,b. Each structure is the result of breaking the chromium–C^6 and –C^7 bonds. Thus, the motion begins with a dissociation that is then followed by coordination of the originally unbound double bond. Both of the estimated transition-state structures have η^4-bound COT rings that resemble the 16-electron complex that Mann predicted.[18] The energy difference between the two structures is large. At the ab initio Hartree–Fock level of theory, IIIb is more stable than IIIa by 23 kcal/mol. The qualitative analysis of the difference between these two structures has already been discussed by Hoffmann and Albright[6k] when they examined the different orientations of the tricarbonyl fragment in $(C_4H_6)(CO)_3Fe$ and the hypothetical molecule $(C_4H_6)(CO)_3Cr$. With polarization d functions on the carbon ring atoms, the activation energy for the 1,3-shift through IIIb is 2.9 kcal/mol. In general, one cannot "bottle" transition states, but in this case, there are several examples of stable 16-electron tricarbonylchromium complexes that adopt the same orientation of the carbonyls as the low-energy 1,3-shift transition state, IIIb. One specific example

(42) Hails, M. J.; Mann, B. E.; Spencer, C. M. *J. Chem. Soc., Dalton Trans.* **1985**, 693.

is tricarbonyl(1,6-methanocyclodecapentaene)chromium.[41] In this molecule, a detailed LMO analysis[40] produced two metal–annulene bonds and therefore a 16-electron complex.

The structure of the COT ring in 111b can be divided into two portions: the four carbons attached to chromium and the four carbons that do not interact with chromium. The C–C bond distances for the carbon atoms not involved in bonding to the metal are 1.32, 1.46, and 1.32 Å for the C^4–C^5, C^5–C^6, and C^6–C^7 bonds, respectively. This portion of the ring clearly resembles butadiene. The C–C bond distances for those atoms that interact with chromium are 1.41, 1.38, and 1.41 Å for the C^8–C^1, C^1–C^1, and C^2–C^1 bonds. These bond lengths are reminiscent of an aromatic ring. The C–C bond lengths in 111b are similar to those in tricarbonyl(butadiene)iron(0)[44] and the appropriate C–C bond lengths in $(COT)(CO)_3Fe$.[45]

The interaction of the COT fragment and the $Cr(CO)_3$ fragment is again a balance between the forward electron donation from COT into the empty d orbitals of $Cr(CO)_3$ and the π back-bonding from the occupied metal d orbitals into the π^* orbitals of the cyclic olefin. As stated above, the portion of the ring that does not interact with Cr is similar to a butadiene fragment. This accounts for two of the four π-electron pairs in the COT ring. The π orbitals of the four carbon atoms that interact with chromium have the nodal characteristics shown in **4**. The 1a′ and 1a″ orbitals are occupied in the fragment. When

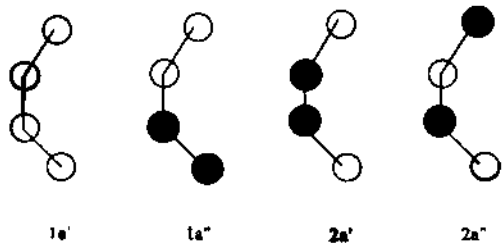

4

COT and $Cr(CO)_3$ unite, the 1a″ and the unoccupied 2a′ orbitals of COT interact strongly with $Cr(CO)_3$. The 1a″ orbital donates charge into the unoccupied a″ orbital of the $Cr(CO)_3$ fragment whereas the 2a′ orbital accepts electrons from $Cr(CO)_3$. The forward donation removes electron density from a C^8–C^1 and C^2–C^1 bonding orbital while decreasing the population of the antibonding C^1–C^1 orbitals. In contrast, the back-bonding populates the C^1–C^1 bonding orbital and the C^8–C^1 and C^1–C^1 antibonding orbital. Both of these effects work to increase the C^1–C^1 bond order and decrease the C^8–C^1 and C^1–C^1 bond orders.

Conclusions

We have calculated a total of nine potential energy surfaces for the ring-shift mechanisms in tricarbonyl(cyclooctatetraene)-chromium(0). The energetics of these reactions were reevaluated at the ab initio Hartree–Fock level by using large metal basis sets. The order of the activation energies for the shift mechanisms is in agreement with the experimental evidence, although our calculated ΔE's are somewhat too low. The bonding was analyzed by dividing the molecule into a COT fragment and a $Cr(CO)_3$ fragment. It was shown that there is a delicate interplay between the COT–Cr bond strength and the distortion energy of the COT ring. The strongest Cr–COT binding did not produce the most stable $(CO)_3(COT)Cr$ complex. This was due to a larger distortion energy, which lowered the overall stability of the complex. The fluxional behavior was shown not to occur via a 20-electron "piano-stool" structure. The 1,5-shift transition state looks like a 1-2:5-6-η-COT) molecule, but in reality only two carbon atoms in the ring form a bond with Cr. Thus, it is a 14-electron, η^1-COT complex. The 1,4-shift transition state is similar to the 1,2-shift transition state except that the carbonyls are rotated 60°. The 1,2-shift proceeds through a transition-state geometry which has an awkward symmetry requirement that does not allow for an alternate single-double-bond arrangement in the COT ring. Nevertheless, a strong Cr–COT bond is formed. The main interaction can be thought of as an allyl group binding to Cr. The 1,3-shift transition state contains an η^4-COT ring, which donates four electrons to the metal, thus producing a 16-electron complex that is structurally very similar to a number of stable 16-electron chromium species. The orientation of the carbonyls is the same as that found in similar η^4-bound, 16-electron chromium complexes.

Acknowledgment. We thank the Robert A. Welch Foundation (Grant No. Y-743), the University of Texas Center for High Performance Computing, and the Texas Advanced Technology Program for support of this work.

Supplementary Material Available: Tables of Cartesian coordinates, Mulliken charges, and degrees of bonding for the ground- and transition-state structures (8 pages). Ordering information is given on any current masthead page.

[41] Baikie, P. E.; Mills, O. S. *J. Chem. Soc. A* **1969**, 128.
[44] Davis, M. I.; Speed, C. S. *J. Organomet. Chem.* **1970**, *21*, 401.
[45] Dickens, B.; Lipscomb, W. N. *J. Chem. Phys.* **1962**, *37*, 2084.